第 41 卷 第 10 期 焊 接 学 报 Vol. 41(10):42 − 46
2020 年 10 月 TRANSACTIONS OF THE CHINA WELDING INSTITUTION October 2020

超声频脉冲电信号耦合前后铝合金 TIG 堆焊接头特点

陈琪昊[1,2]， 崔山成[1]， 林三宝[2]， 高翔[1]， 张澳[1]
(1. 江苏科技大学, 镇江, 212100; 2. 哈尔滨工业大学, 先进焊接与连接国家重点实验室, 哈尔滨, 150001)

摘要: 电弧堆焊作为一种低成本高效率的焊接方法在材料表面修复领域具有广阔的应用前景, 文中将超声频脉冲电信号与低频交流 TIG 焊接电信号耦合, 将超声能量引入 TIG 堆焊过程, 改善铝合金 TIG 堆焊质量. 对超声频脉冲电信号耦合前后 5083 铝合金 TIG 堆焊焊缝成形、组织及硬度进行对比. 结果表明, 随超声电源输出电压的增大, 焊缝成形向熔宽减小、余高增大的趋势变化. 超声作用后, 晶粒尺寸发生了一定变化, 但晶粒形态无明显变化. 熔合区的晶粒细化最显著; 焊缝区及热影响区的晶粒细化不明显, 相反, 随超声电源输出电压的增大, 晶粒明显粗化. 熔合区及热影响区的第二相分布呈聚集现象. 超声作用对晶粒内部 Mg 元素的分布影响较大, 增大超声电源输出电压, Mg 元素在晶界处的偏析减弱. 硬度测试结果表明, 超声频脉冲电信号耦合后焊缝硬度增大.

关键词: 超声频电信号; 电弧; 焊缝成形; 组织
中图分类号: TG 442, TG 444 **文献标识码:** A **doi:** 10. 12073/j. hjxb. 20200312001

0 序言

复合的电弧焊接技术 (如等离子弧-电弧复合焊接[1] 及超声-电弧复合焊接[2]), 通过在传统电弧能场中引入附加能场可有效改善电弧焊接质量. 其中超声电弧复合焊接方法可以改善电弧形态、熔滴过渡及焊缝组织[3-4], 可有效改善焊接接头的力学性能. 超声-电弧复合焊接方法主要包括机械施加式和电耦合式两种, 与机械施加式复合焊接方法[5-8] 相比, 电耦合式电弧超声焊接方法[9] 的应用不受焊接工件尺寸及焊炬结构的限制, 焊接场所适应性强, 具有较好的应用前景.

已有研究主要侧重于电弧超声能量对焊接质量的影响以及电弧超声能量的影响因素. 研究表明, 电弧的超声振动存在谐振频率[10], 超声激励电流是影响电弧超声强度的主要因素[11-12]. 电弧超声可改善焊缝成形、细化焊缝组织、减小偏析、提高接头力学性能[13-14]. 电弧超声由于通过电耦合方式向焊接过程引入超声能量, 会引入附加的超声热输入, 附加热输入过大会导致接头晶粒粗化, 因此, 附加超声热输入的控制对焊缝晶粒尺寸具有重要的影响. 目前关于电弧超声附加热输入的影响未见具体研究.

铝合金电弧堆焊技术在材料表面修复领域具有重要的应用价值及广阔的应用前景. 许凯等人[15] 研究了旋转磁场对 ZL205A MIG 堆焊层组织及性能的影响, 研究表明旋转磁场可使堆焊层的晶粒细化, 并且提高焊缝硬度. Chen 等人[16] 通过机械耦合的方式将脉冲超声引入 GMAW 过程, 研究了脉冲超声对 Al-Cu 合金 MIG 堆焊质量的影响, 结果表明施加脉冲超声后熔滴过渡模式改变, 并且焊缝柱状晶区域减小. 尽管通过旋转磁场及机械超声的方式可以细化铝合金电弧堆焊的焊缝晶粒、提高堆焊接头性能, 但焊炬比较复杂, 导致其应用受到一定限制.

5083 铝合金广泛应用于船舶与海洋工程, 其 TIG 堆焊焊缝存在组织粗大及组织不均匀等问题. 基于电弧超声辅助焊接方法的优势, 针对 5083 铝合金 TIG 堆焊存在的不足, 通过在 TIG 焊接电信号中耦合超声频脉冲电信号, 激发电弧产生超声振动, 作用于熔池, 进而改善堆焊质量. 通过研究, 揭示超声频脉冲电信号作用后, 铝合金 TIG 堆焊焊缝成形、组织及力学性能的变化, 进而为铝合金堆焊工艺优化提供指导.

1 焊接装置及方法

焊接装置示意图如图 1 所示, 超声电源与 TIG

收稿日期: 2020 − 03 − 12
基金项目: 国家自然科学基金资助项目 (51905230); 先进焊接与连接国家重点实验室开放课题研究基金资助 (AWJ-20-M06).

焊接电源通过隔离耦合装置并联，将超声频脉冲电信号与低频的 TIG 电信号进行耦合，调制焊接电信号产生高频特性，进而将超声能量引入焊接过程，改善焊缝成形、组织及力学性能. 超声电源输出交变矩形脉冲电信号，正负脉宽相等，超声电源的输出频率为 20 kHz. 焊接电源采用交流焊接模式. 焊接采用堆焊方法进行，母材为 4 mm 厚度的 5083 铝合金，焊丝采用直径 1.2 mm 的 ER5183 铝合金焊丝. 焊接电流为 140 A，送丝速度为 0.6 m/min，焊接速度为 90 mm/min.

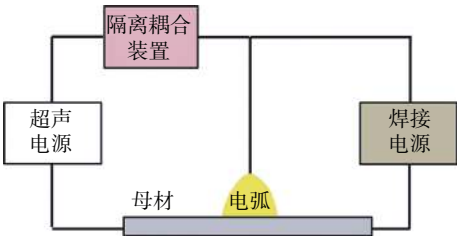

图 1　焊接装置示意图

Fig. 1　Schematic diagram of welding device

利用金相显微镜对焊缝宏观形貌进行拍摄，并利用 Image-Pro Plus 软件对表征焊缝成形相关的物理量进行测量. 利用 SEM 及 EBSD 表征手段对焊缝组织进行表征，分析元素分布、第二相分布及晶粒特征的变化. 利用硬度计对焊缝硬度进行表征分析. 焊缝形貌特征及硬度测试位置如图 2 所示，硬度测试位置位于焊缝中间部位.

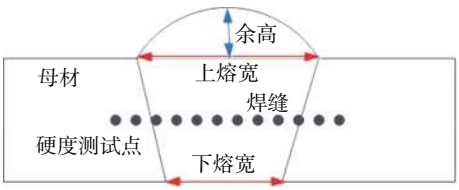

图 2　焊缝形貌特征及硬度测试位置示意图

Fig. 2　Schematic diagram of weld appearance and hardness measurement positions

2　试验结果

2.1　焊缝宏观形貌

不同超声电压下的焊缝宏观成形特征如图 3 所示，对上熔宽、下熔宽及余高进行测量统计，可以看出，在相同的焊接参数下，当超声电压为 100 V 时，焊缝上熔宽及下熔宽均明显减小，余高明显增大. 随着超声电压的增大，焊缝宏观形貌向熔宽减小、余高增大的趋势变化.

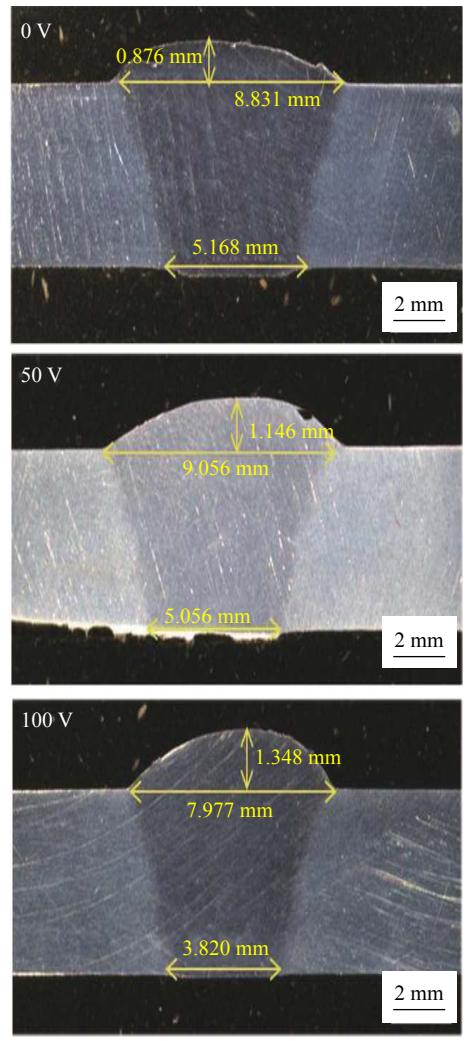

(a) 焊缝宏观形貌

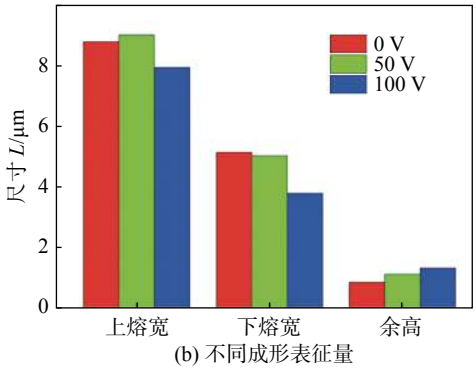

(b) 不同成形表征量

图 3　焊缝宏观形貌及参数统计

Fig. 3　Macroscopic appearance of weld and parameter statistics. (a) macroscopic appearance of weld; (b) statistics of weld formation parameters

2.2　焊缝组织

对接头晶粒特征、第二相分布及元素偏析进行分析，图 4 为焊缝区、熔合区及热影响区晶粒特征，可以看出，超声频脉冲电信号作用前后接头各区域的晶粒形态没有发生明显变化，晶粒形态均为等轴

晶形态. 然而, 各区域的晶粒尺寸发生了明显变化. 图 5 为不同超声电压下的焊缝区、熔合区及热影响区晶粒尺寸, 从图中可以看出, 对于焊缝区, 超声频脉冲电信号耦合后, 晶粒尺寸没有发生明显细化, 当超声电压为 100 V 时出现了晶粒粗化现象. 对于熔合区, 超声频脉冲电信号耦合后, 晶粒尺寸发生明显细化, 当超声电压为 100 V 时, 尽管晶粒尺寸小于无超声时的晶粒尺寸, 但是与超声电压为 50 V 情况相比, 细化程度明显下降. 对于热影响区, 超声频脉冲电信号耦合后, 晶粒没有细化, 反而出现了粗化, 与无超声耦合情况相比, 随超声电压的增大, 热影响区晶粒尺寸逐渐增大.

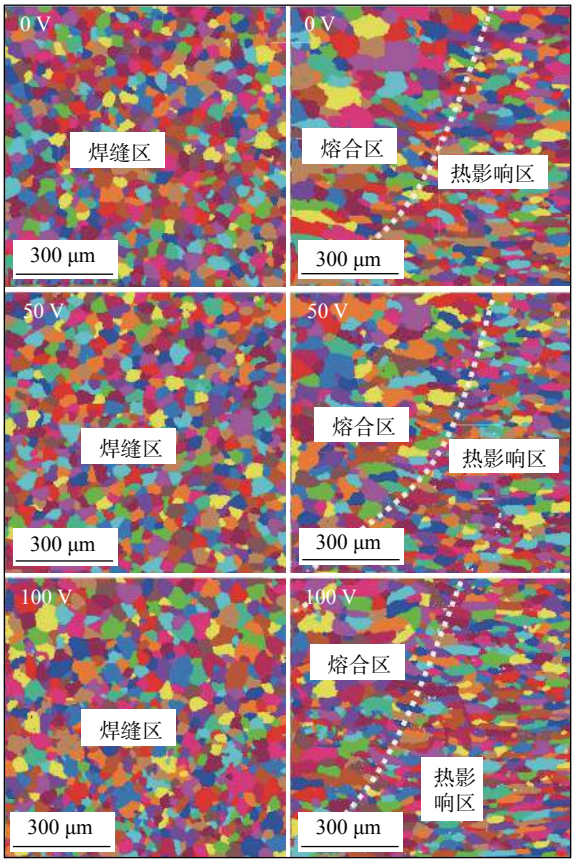

图 4 不同超声电压下的接头晶粒特征

Fig. 4 Grain characteristics in welded joints with different ultrasonic voltages

超声作用于 5083 铝合金 TIG 堆焊, 对焊缝区、熔合区及热影响区晶粒具有不同的影响规律. 超声对熔合区晶粒细化作用最显著; 焊缝区及热影响区晶粒没有明显细化, 当超声电压较高时晶粒粗化. 分析认为, 电弧超声同时存在两种效应, 分别为超声振动效应及附加热效应, 两种效应对晶粒细化作用是矛盾的. 超声振动效应可通过促进熔池内晶粒

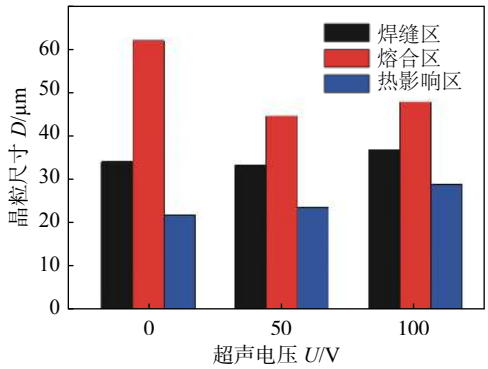

图 5 不同超声电压下的接头晶粒尺寸

Fig. 5 Grain size in welded joints with different ultrasonic voltages

的异质形核细化晶粒[17], 然而附加热效应却可使焊接区域温度增大导致晶粒长大. 随超声电压增大, 热效应的影响逐渐增大, 导致晶粒细化效果逐渐减弱, 当附加热效应的影响超过超声振动的影响时, 晶粒细化现象消失. 对于热影响区, 超声振动效应影响较小, 主要为热效应的影响, 因此, 电弧超声对热影响区晶粒细化无明显作用.

图 6 ~ 图 8 分别为焊缝中心、熔合区及热影响区第二相分布特征, 从图中可以看出, 焊缝中心处, 不同超声电压作用下, 第二相分布没有发生明显变化.

在熔合区及热影响区, 当超声电压为 50 V 及 100 V 时, 第二相尺寸明显增大, 表现为聚集特征. 此结果表明, 电弧超声的热效应对熔合区及热影响区第二相分布具有不利的影响. 超声频脉冲电信号耦合后, 由于热冲击作用, 熔合区及热影响区第二相尺寸增大[18].

焊缝区元素分布统计结果如图 9 所示, 结果表明, 超声频脉冲电信号作用对晶粒内部 Mg 元素分布影响较大, 超声频脉冲电信号作用后, 可有效减小 Mg 元素在晶界处的偏析程度. 5083 铝合金中主要的合金元素为 Mg 元素, Mg 元素的分布对焊接质量具有直接的影响, 电弧超声作用下熔池内产生超声空化及声流效应, 促进了 Mg 元素向固相中的扩散, 从而减小了 Mg 元素的微观偏析.

2.3 接头硬度

图 10 为不同参数下的接头硬度分布情况, 结果表明, 超声频脉冲电信号耦合后, 接头各区域硬度均有所提高, 其中, 超声电压为 50 V 时, 接头硬度要明显高于超声电压为 100 V 时的接头硬度.

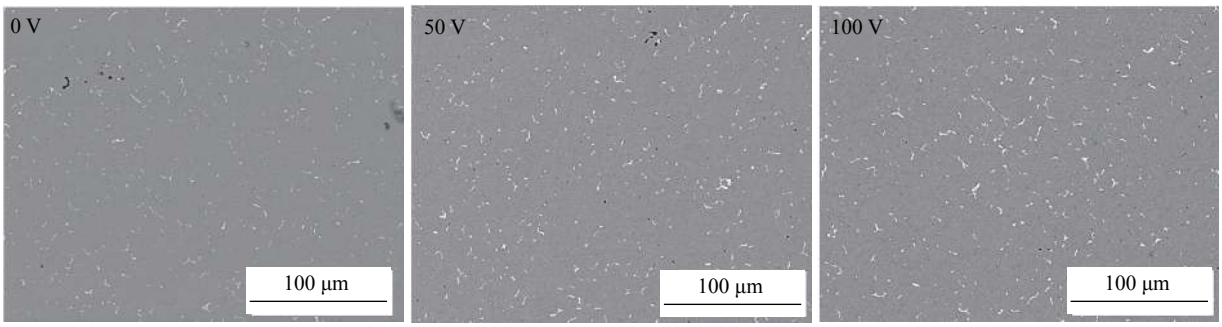

图 6　不同超声频电压下的焊缝中心第二相分布

Fig. 6　Second phase distribution in weld center with different ultrasonic voltages

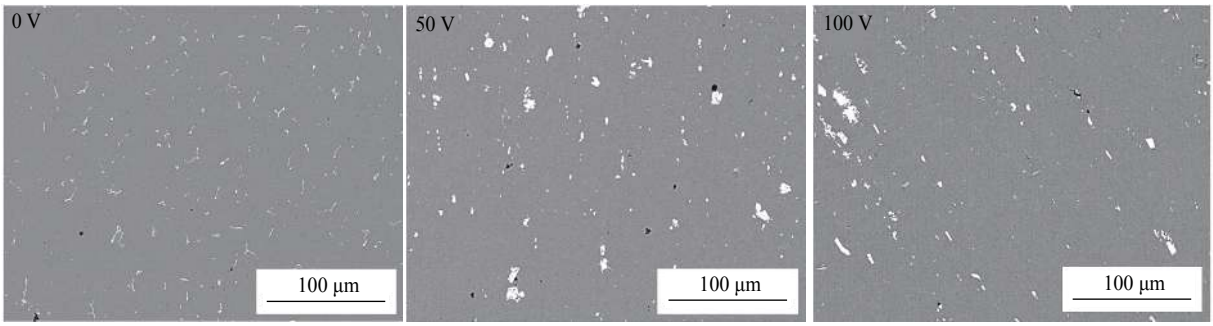

图 7　不同超声频电压下熔合区第二相分布

Fig. 7　Second phase distribution in fusion zone with different ultrasonic voltages

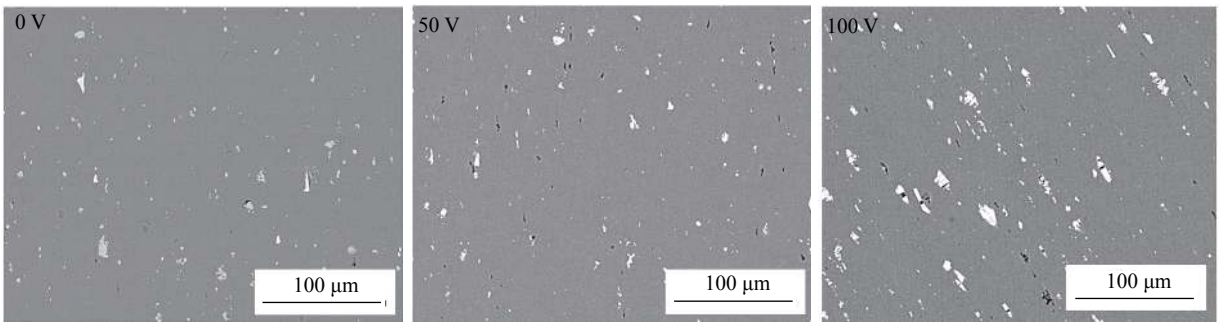

图 8　不同超声频电压下热影响区第二相分布

Fig. 8　Second phase distribution in heat affected zone with different ultrasonic voltages

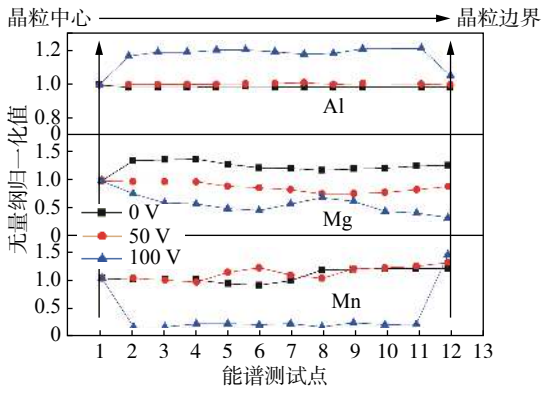

图 9　焊缝中心晶粒内部元素分布

Fig. 9　Element distribution in grain in weld center

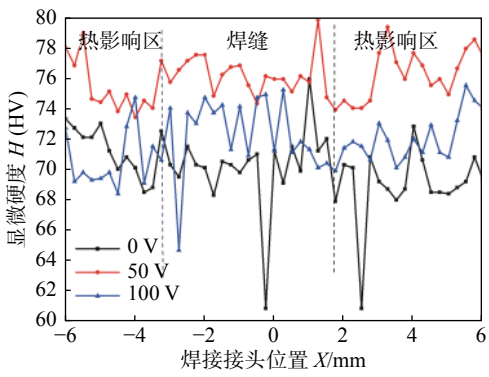

图 10　接头硬度分布

Fig. 10　Hardness distribution in welded joint

3 结论

(1) 超声频脉冲电信号耦合可改变焊缝宏观成形, 随超声频脉冲电信号电压增大, 焊缝成形向熔宽减小、余高增大的趋势变化.

(2) 超声作用后, 焊缝组织特征发生明显变化: 熔合区晶粒明显细化; 熔合区及热影响区第二相聚集; 超声作用对晶粒内部 Mg 元素分布影响较大, 增大超声电压, Mg 元素在晶界附近的偏析程度减弱.

(3) 超声作用后, 接头焊缝区及热影响区硬度均有所提高, 当超声输入电压为 50 V 时, 接头硬度提高最大.

参考文献

[1] Wang Y J, Wei B, Guo Y Y, *et al*. Microstructure and mechanical properties of the joint of 6061 aluminum alloy by plasma-MIG hybrid welding[J]. China Welding, 2017, 26(2): 58 − 63.

[2] Wang D Q, Hua C, Lu H. Numerical analysis of ultrasonic waves in the gas tungsten arc welding (GTAW) with ultrasonic excitation of current[J]. International Journal of Heat and Mass Transfer, 2020, 158: 1 − 10.

[3] Chen C, Fan C L, Cai X X, *et al*. Characteristics of arc and metal transfer in pulsed ultrasonic-assisted GMAW[J]. Welding Journal, 2020, 99(7): 203s − 208s.

[4] Fattahi M, Ghaheri A, Arabian N, *et al*. Applying the ultrasonic vibration during TIG welding as a promising approach for the development of nanoparticle dispersion strengthened aluminum weldments[J]. Journal of Materials Processing Technology, 2020, 282: 116672.

[5] Chen C, Fan C L, Liu Z, *et al*. Microstructure evolutions and properties of Al–Cu alloy joint in the pulsed power ultrasonic-assisted GMAW[J]. Acta Metallurgica Sinica (English Letters), 2020, 33(10): 1397 − 1406.

[6] Dong H G, Yang L Q, Dong C, *et al*. Improving arc joining of Al to steel and Al to stainless steel[J]. Materials Science and Engineering A, 2012, 534: 424 − 435.

[7] Watanabe T, Shiroki M, Yanagisawa A, *et al*. Improvement of mechanical properties of ferritic stainless steel weld metal by ultrasonic vibration[J]. Journal of Materials Processing Technology, 2010, 210(12): 1646 − 1651.

[8] Yuan T, Kou S, Luo Z. Grain refining by ultrasonic stirring of the weld pool[J]. Acta Materialia, 2016, 106: 144 − 154.

[9] 雷玉成, 崔展祥, 路广遥, 等. 超声电弧对 6061 铝合金 MIG 焊接头组织和性能的影响 [J]. 焊接学报, 2020, 41(2): 33 − 38.
Lei Yucheng, Cui Zhanxiang, Lu Guangyao, *et al*. Effect of arc-ultrasonic on the microstructure and properties of 6061 aluminum alloy joint with MIG welding[J]. Transactions of the China Welding Institution, 2020, 41(2): 33 − 38.

[10] 吴敏生, 段向阳, 李路明, 等. 电弧超声的激发及其特性研究 [J]. 清华大学学报 (自然科学版), 1999, 39(6): 110 − 112.
Wu Minsheng, Duan Xiangyang, Li Luming, *et al*. Study of arc-ultrasonic excitation and its characteristics[J]. Journal of Tsinghua University (Science & Technology), 1999, 39(6): 110 − 112.

[11] He L B, Yang P, Li L M, *et al*. The ultrasonic characteristics of high frequency modulated arc and its application in material processing[J]. Ultrasonics, 2014, 54(8): 2178 − 2183.

[12] 张春雷, 吴敏生. 高频调制电弧超声发射及其物理特性 [J]. 焊接学报, 2001, 22(1): 75 − 78.
Zhang Chunlei, Wu Minsheng. High-frequency modulated arc as an ultrasonic generator and its physical property[J]. Transactions of the China Welding Institution, 2001, 22(1): 75 − 78.

[13] Chen X Z, Shen Z, Wang J J, *et al*. Effects of an ultrasonically excited TIG arc on CLAM steel weld joints[J]. International Journal of Advanced Manufacturing Technology, 2012, 60(5−8): 537 − 544.

[14] Qi B J, Yang M X, Cong B Q, *et al*. The effect of arc behavior on weld geometry by high-frequency pulse GTAW process with 0Cr18Ni9Ti stainless steel[J]. International Journal of Advanced Manufacturing Technology, 2013, 66(9−12): 1545 − 1553.

[15] 许凯, 侯击波, 刘雅鑫, 等. 旋转磁场对 ZL205A 堆焊层组织与性能的影响 [J]. 热加工工艺, 2019, 48(7): 69 − 72.
Xu Kai, Hou Jibo, Liu Yaxin, *et al*. Influence of rotating magnetic field on microstructure and properties of ZL205A aluminum alloys surfacing layer[J]. Hot Working Technology, 2019, 48(7): 69 − 72.

[16] Chen C, Fan C L, Cai X Y, *et al*. Analysis of droplet transfer, weld formation and microstructure in Al-Cu alloy bead welding joint with pulsed ultrasonic-GMAW method[J]. Journal of Materials Processing Technology, 2019, 271: 144 − 151.

[17] 陈琪昊, 林三宝, 杨春利, 等. 超声作用阶段及形式对熔池晶粒结晶的影响 [J]. 焊接学报, 2020, 41(3): 29 − 32.
Chen Qihao, Lin Sanbao, Yang Chunli, *et al*. Effect of different ultrasonic action stages on grain crystallization in TIG weld pool[J]. Transactions of the China Welding Institution, 2020, 41(3): 29 − 32.

[18] 金礼, 徐敏, 薛家祥, 等. 热输入对铝合金双脉冲 MIG 焊接头性能的影响 [J]. 焊接学报, 2018, 39(1): 89 − 92.
Jin Li, Xu Min, Xue Jiaxiang, *et al*. Effect of line energy on properties of aluminum alloy joints in double pulsed MIG welding[J]. Transactions of the China Welding Institution, 2018, 39(1): 89 − 92.

第一作者简介: 陈琪昊, 1988 年出生, 博士; 主要从事铝合金电弧焊研究工作; Email: qhchen@just.edu.cn.

（编辑： 高忠梅 ）

Microstructures and mechanical properties of the welded joint were investigated. Energy disperse spectroscopy (EDS) was used to measure the burning loss of alloy elements in different regions of the weld. The tensile strength and microhardness of the weld were also measured. The results showed microstructures in the upper area were smaller than that in the lower area, the content of Mg and Zn in the upper part of weld was lower than that in the lower edge. Microhardness in the upper center was higher than that in the lower center, while microhardness at the upper edge was smaller than that at the lower edge. A ductile fracture was observed as the key characteristic for the welded joint, and the tensile strength was 325 MPa, of 65.9% of base metal. The decrease of the tensile strength was caused by the burning loss of Mg, Zn, welding stresses and porosity defects.

Key words: 7A52 alloy; laser beam welding; microstructure; mechanical properties

Microstructure and properties analysis of Incoloy 825 nickel base alloy electron beam welding ZHANG Jianxiao[1,2], GUAN Zhichen[1], HUANG Jiangkang[1], YANG Zhihai[3], FAN Ding[1] (1. State Key Laboratory of Advanced Processing and Recycling of Non-ferrous Metals, Lanzhou University of Technology, Lanzhou, 730050, China; 2. Lanzhou LS Heavy Equipment Co., LTD., Lanzhou, 730314, China; 3. Lanzhou Changzheng Machinery Co., LTD., Lanzhou, 730299, China). pp 32-37

Abstract: The butt test of Incoloy 825 nickel base superalloy in air cooler tube box was studied by electron beam welding. The microstructure of electron beam welded joints was analyzed by observing the structure of welded joints, and the mechanical properties of electron beam welded joints were analyzed with tensile properties and impact toughness tests. The results show that good weld joint of lncoloy 825 alloy can be obtained by electron beam welding. The weld zone is composed of large equiaxed grains and a few columnar crystals. There is no obvious element loss in the we4ld area. The hardness of weld and heat affected zone reaches the hardness value of base metal. The tensile strength of the weld joint reaches 600 MPa, which is close to the tensile strength of the base metal, and the fracture form of the joint is ductile fracture. The impact value in the weld and heat affected zone is higher than that of the base metal, in which the impact energy in the weld joint reaches 262 J, and the impact fracture morphology is ductile fracture.

Key words: electron beam welding; Incoloy 825; microstructure; mechanical property

Effect of ultrasonic impact treatment on corrosion behavior of FSW joints of 2A12 aluminum alloy ZHANG Timing[1], DENG Yunfa[1], CHEN Yuhua[1], FANG Yu[2], HU Xuebing[3] (1. Nanchang Hangkong University, Nanchang, 330063, China; 2. Shanghai Aerospace Equipments Manufacturer, Shanghai, 200245, China; 3. Sino-Pipeline International Co., Ltd., Beijing, 100007, China). pp 38-41,78

Abstract: In this work, the corrosion behavior of friction stir welding (FSW) joints of 2A12 aluminum alloy with and without ultrasonic impact treatment (UIT) was investigated by immersion corrosion test and polarization curve test in 3.5% NaCl aqueous solution. The results showed that the average corrosion rate of the joints with UIT was about half of that without UIT. The corrosion potential of the heat affected zone (HAZ) without UIT was −0.629 V (Ag/AgCl), indicating the worst corrosion resistance. And the average corrosion depth of HAZ induced by pitting corrosion and intergranular corrosion was about 125 μm. After UIT, the corrosion potentials of each sub-area of the FSW joints increased, and the corresponding corrosion current density decreased. The maximum depth of corrosion pit did not exceed 40 μm. The whole surface of the joint exhibited a form of uniform corrosion. Ultrasonic impact makes the surface grains of the material finer and denser, and the bond between the strengthening phase and the base metal is tighter, which is the main reason for the improvement of the corrosion resistance of the material. The main reason for the improvement of the corrosion resistance of the joints was that the grains of the material were refined and densified after UIT.

Key words: 2A12 aluminum alloy; friction stir welding; ultrasonic impact treatment; corrosion behavior

Characteristics of TIG overlaying welded joints of aluminum alloy before and after implementing ultrasonic frequency pulse electric signal CHEN Qihao[1,2], CUI Shancheng[1], LIN Sanbao[2], GAO Xiang[1], ZHANG Ao[1] (1. Jiangsu University of Science and Technology, Zhenjiang, 212100, China; 2. State Key Laboratory of Advanced Welding and Joining, Harbin Institute of Technology, Harbin, 150001, China). pp 42-46

Abstract: As a low-cost and high-efficiency welding method, arc overlaying welding has a broad application

prospect in the field of material surface repair. In this study, ultrasonic energy is introduced into the TIG overlaying process to improve the welding quality of aluminum alloy by coupling the ultrasonic frequency pulse electrical signal with the low-frequency AC TIG welding electrical signal. The weld formation, microstructure, and hardness of overlaying welded joints of 5083 aluminum alloy were compared before and after implementing an ultrasonic pulse electrical signal. The results show that the weld formation changes towards the trend of decreased fusion wide and increased surplus height with the increase of the output voltage of the ultrasonic power. The grain size changs to some extent, but the grain morphology changs little after implementing the ultrasonic treatment. Grain refinement is the most significant in the fusion zone, but it is not obvious in the weld zone and the heat-affected zone. On the contrary, grain coarsening is obvious with the increase of the output voltage of the ultrasonic power. The distribution of the second phase in the fusion zone and the heat-affected zone shows an aggregation phenomenon. The ultrasonic effect has a great influence on the distribution of Mg element inside the grain. The segregation degree of Mg element at the grain boundary could be weakened by increasing the output voltage of the ultrasonic power. The hardness test results show that the weld hardness increases after coupling the ultrasonic frequency pulse electrical signal.

Key words: ultrasonic frequency electrical signal; arc; weld formation; microstructure

Microstructure and properties of plasma arc additive repairing depositions for the worn rotor journal of power station equipment GUO Yang[1,2], ZHANG Jianxun[1], XIONG Jiankun[2], LIU Yan[1], ZHAO Pengfei[2] (1. State Key Laboratory for Mechanical Behavior of Materials, Xi 'An Jiaotong University, Xi 'an, 710049, China; 2. State Key Laboratory of Long-Life High Temperature Materials, Dongfang Electric Corporation Dongfang Turbine Co.,Ltd., Deyang, 618000, China). pp 47-53

Abstract: In view of the in situ repairing requirements of rotor journal of power plant equipment, a non preheating single-layer and multi-passes additive depositing 316L alloy was achieved on 20Cr2NiMo steel by Micro Plasma Arc Depositing process. The microstructure, hardness, chemical composition and mechanical properties of deposition and heat affected zone were analyzed. The results show that the deposition is metallurgical bonded with the substrate, and there is no crack in the cladding layer and heat affected zone; the microstructure of 316L deposition consists of austenite + δ ferrite, and the primary heat affected zone can be divided into decarburization zone, coarse-grained zone, fine-grained zone and mixed crystalline zone, and the primary coarse-grained zone is coarsened, refined and softened due to the secondary heat cycle. The difference of hardness between 316L deposition and substrate is small, while the hardness of primary coarse-grained zone is the highest, but that of secondary coarse-grained zone below 476HV0.3, and the width of heat affected zone is about 2.5 mm; the shear strength of heat affected zone is higher than that of substrate, but the plasticity of substrate is better.

Key words: rotor journal; micro plasma arc depositing process; interface; in situ repairing; shear strength

Microstructure and properties of low voltage electron beam wire deposition layer of TC4 titanium alloy WANG Ting[1,2], WANG Yifan[1], WEI Lianfeng[3], LI Qixian[1], JIANG Siyuan[1] (1. State Key Laboratory of Advanced Welding and Joining, Harbin Institute of Technology at Weihai, Weihai, 264209, China; 2. Shandong Provincial Key Laboratory of Special Welding Technology, Harbin Institute of Technology at Weihai, Weihai, 264209, China; 3. Science and Technology on reactor Nuclear Power Institute of China, Chengdu, 610041, China). pp 54-59

Abstract: The low voltage electron beam wire deposition tests on TC4 titanium alloy were carried out to explore the feasibility of the method, and the influence of the number of deposited layers on the microstructure and properties was analyzed. The results show that the multi-layer wire deposition of TC4 titanium alloy can also be completed on the accelerated voltage of 10 kV. The average microhardness of the deposited parts after multi-layer deposition is about 260 HV, and only the microhardness of the banded texture at the bottom of the deposited parts is close to 288 HV of the annealed TC4 substrate. Banded texture produced in multi-layer deposition process, β phase grain transformed to α + α′ + β by the influence of thermal cycle, the banded texture which composited with basket-like α′ phase and lamellar α phase have high microhardness, the other feature of banded texture is that more basket-like phase gradually integrated into the lamellar structure as the increase of the distance with substrate. The tensile fracture of the deposited part is also ductile fracture with the maximum tensile strength of 862 MPa, which is slightly